CHEMISTRY OF MATERIALS

ARTICLE

pubs.acs.org/cm

Functionalization of Borate Networks by the Incorporation of Fluoride: Syntheses, Crystal Structures, and Nonlinear Optical Properties of Novel Actinide Fluoroborates

Shuao Wang,[†] Evgeny V. Alekseev,*[,†,‡] Juan Diwu,[†] Hannah M. Miller,[†] Allen G. Oliver,[†] Guokui Liu,[§] Wulf Depmeier,[‡] and Thomas E. Albrecht-Schmitt*[,†]

[†]Department of Civil Engineering and Geological Sciences and Department of Chemistry and Biochemistry, University of Notre Dame, 156 Fitzpatrick Hall, Notre Dame, Indiana 46556, United States

[‡]Institut für Geowissenschaften, Universität zu Kiel, 24118 Kiel, Germany

[§]Chemical Sciences and Engineering Division, Heavy Elements and Separation Science, Argonne National Laboratory, Argonne, Illinois 60439, United States

Supporting Information

ABSTRACT: The boric acid flux reactions of uranyl nitrate with sodium, potassium, rubidium, or thallium fluoride result in the formation of a novel family of uranyl(VI) fluoroborate materials. These compounds are $Na[(UO_2)B_5O_8(OH)F]\cdot H_2O$ (**NaUBOF-1**), $K[(UO_2)B_5O_8(OH)F]$ (**KUBOF-1**), $K_{11}[(UO_2)_6B_{24}O_{36}F_{22})](H_2BO_3)$ (**KUBOF-2**), $Rb[(UO_2)B_5O_8(OH)F]$ (**RbUBOF-1**), and $Tl[(UO_2)B_5O_8(OH)F]$ (**TlUBOF-1**). A new neptunium(VI) fluoroborate that is isotypic with **NaUBOF-1**, $Na[(NpO_2)B_5O_8(OH)F]\cdot H_2O$ (**NaNpBOF-1**), was synthesized via the boric acid flux reaction of neptunium(VI) nitrate with sodium fluoride. These new actinide fluoroborates share a common structural motif consisting of a linear actinyl ($U(Np)O_2^{2+}$) cation surrounded by BO_3 triangles and BO_4 tetrahedra to create an $U(Np)O_8$ hexagonal bipyramidal environment around uranium or neptunium. The borate anions bridge between actinyl units to create layers. B−F bonds were formed during the reactions to yield BO_3F tetrahedral units. The BO_3F tetrahedra and additional BO_3 triangles extend from the actinyl polyborate layers and are directed approximately perpendicular to the layers. A novel actinyl borate layered topology was found in $K_{11}[(UO_2)_6B_{24}O_{36}F_{22})](H_2BO_3)$ (**KUBOF-2**). Except for $K[(UO_2)B_5O_8(OH)F]$ (**KUBOF-1**) and $K_{11}[(UO_2)_6B_{24}O_{36}F_{22})](H_2BO_3)$ (**KUBOF-2**), all of the other actinide fluoroborate phases adopt noncentrosymmetric space groups. $Tl[(UO_2)B_5O_8(OH)F]$ (**TlUBOF-1**), which can be obtained as a pure phase, displays second-harmonic generation of 532-nm light from 1064-nm light.

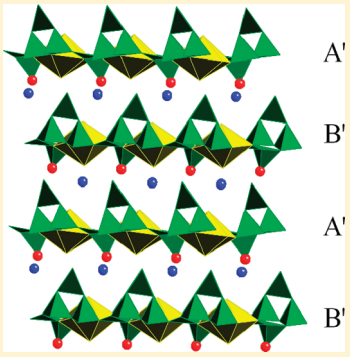

KEYWORDS: actinide borate, uranium borate, neptunium borate, fluoroborate, noncentrosymmetric materials, nonlinear optical materials

INTRODUCTION

The nonlinear optical applications of borate materials have been heavily investigated over the past several decades.[1] β-BaB_2O_4 (BBO) is one of earliest and best developed examples,[1a] and improved second-harmonic generation have been realized other materials such as α-BiB_3O_6.[2] The success of these borate crystals can be largely attributed to the unique structural characteristics of borate building units, since the most common borate units are BO_3 triangles and BO_4 tetrahedra, and neither of these units can possess an inversion center. In a typical polyborate structure, BO_3 triangles and BO_4 tetrahedra share corners to form larger polyborate clusters, although rare examples of edge-sharing by two BO_4 tetrahedra have been found.[3,4] Because there are a vast number of different topological arrangements of the polyborate clusters, the solid-state and materials chemistry of borates is very rich.[5,6]

One of the least explored borate systems is the actinide borates.[7−14] We recently adopted the boric acid flux synthetic technique to synthesize a thorium borate, $[ThB_5O_6(OH)_6][BO(OH)_2]\cdot 2.5H_2O$ (**NDTB-1**), with a cationic framework structure and remarkable anion exchange capabilities,[15,16] a large family of uranyl borates,[17−20] several neptunium borates with variety of combinations of single valence states or mixed/intermediate valence states, and a single plutonium(VI) borate.[21−24] In particular, a significant percentage of these uranyl borates adopt noncentrosymmetric structures, and these compounds may aid in the design of other nonlinear optical materials.[17−20] Among the 21 uranyl borates that we have already reported, 13 of them adopt noncentrosymmetric space groups.[17−20] $Li[(UO_2)B_5O_9]\cdot H_2O$, $Na[(UO_2)B_6O_{10}]\cdot 2H_2O$, $K[(UO_2)_2B_{10}O_{16}(OH)_3]\cdot H_2O$, and β-$Tl_2[(UO_2)_2B_{11}O_{18}(OH)_3]$, which can be obtained as pure phases, display second-harmonic generation of 532-nm light from 1064-nm light.[17−20]

Received: February 16, 2011
Revised: May 2, 2011
Published: May 13, 2011

dx.doi.org/10.1021/cm2004984 | *Chem. Mater.* 2011, 23, 2931–2939

The term "fluoroborate" is predominantly represented by the tetrafluoroborate anion BF_4^-, which often acts as an out-sphere, charge-balancing anion. However, fluoroborates have been largely expanded by the recent observations of partial substitution of O atoms by F atoms in the BO_4 units to form BOF_3^{2-}, $BO_2F_2^{3-}$, or BO_3F^{4-} anions.[25−30] The first example of BOF_3^{2-} was shown in the structure of $BaBOF_3$, but the bond distance information turns out to be very suspicious.[25] A more reliable description of the $BO_2F_2^{3-}$ anion first appeared in an organically templated borophosphate compound, $(C_2H_{10}N_2)[BPO_4F_2]$, where reasonable evidence for the partial substitution of O atoms by F atoms in the BO_4 units was shown.[26] Finally, the BO_3F^{4-} unit was first reported in the compound $NH_4[BPO_4F]$,[27] and was rapidly expanded in the structures of $NH_4[BAsO_4F]$,[28] BiB_2O_4F,[29] and LiB_6O_9F.[30] In these compounds, B−F bonds are reasonably shorter than the B−O bonds in the same BO_3F^{4-} units, which can be used as evidence for identifying the presence of F^- in the structures.

We started to consider actinide fluoroborate compounds for several reasons. First, compared to the BO_4 tetrahedra, the partial substitution of O atoms by F atoms will further reduce the symmetry; thus, a noncentrosymmetric structure could yield a larger nonlinear optical response, based on the polarization of the B−F bond. Actually, except for $BaBOF_3$, whose description is questionable, all of the aforementioned fluoroborate compounds crystallize in noncentrosymmetric space groups.[26−30] Second, compared to oxide anions, F^- anions are more likely to be terminal instead of bridging; thus, the incorporation of fluoride can be used to functionalize the structure of actinide borate sheets and frameworks, and novel actinide borate topologies should be observed. Finally, the redox chemistry of transuranium borates could be affected by further incorporation of fluoride. In this paper, we will describe the syntheses, structures, and properties of a novel actinide fluoroborate family, and how these goals are realized.

EXPERIMENTAL SECTION

Syntheses. $UO_2(NO_3)_2\cdot 6H_2O$ (98%, International Bio-Analytical Industries), $^{237}NpO_2$ (99.9%, Oak Ridge, $t_{1/2} = 2.14 \times 10^6$ yr, made by the oxidation of triple electro-refined Np metal), H_3BO_3 (99.99%, Alfa-Aesar), NaF (99%, Alfa-Aesar), KF (99%, Acros), $RbF\cdot xH_2O$ (99%, Alfa-Aesar), and TlF (99%, Strem) were used as received without further purification. Distilled and Millipore filtered water with a resistance of 18.2 MΩ cm was used in all reactions. Polytetrafluorethylene (PTFE)-lined autoclaves were used for all reactions. *Caution! ^{237}Np ($t_{1/2} = 2.14 \times 10^6$ y) represents a serious health risk, because of its α- and γ-emissions, and especially because of its decay to the short-lived isotope ^{233}Pa ($t_{1/2} = 27.0$ d), which is a potent β- and γ-emitter. All studies with neptunium were conducted in a laboratory dedicated to studies on transuranium elements. This laboratory is located in a nuclear science facility and is equipped with HEPA-filtered hoods and negative pressure gloveboxes that are ported directly into the hoods. A series of counters continually monitor radiation levels in the laboratory. The laboratory is licensed by the Nuclear Regulatory Commission. All experiments were carried out with approved safety operating procedures. All free-flowing solids are handled within gloveboxes, and products are only examined when coated with either water or Krytox oil and water. There are significant limitations in accurately determining yield with neptunium compounds, because this requires drying, isolating, and weighing a solid, which poses certain risks, as well as manipulation difficulties, given the small quantities employed in the reactions.*

Synthesis of $Na[(UO_2)B_5O_8(OH)F]\cdot H_2O$ (NaUBOF-1). $UO_2(NO_3)_2\cdot 6H_2O$ (0.1000 g, 0.2 mmol), boric acid (0.2720 g, 4.4 mmol), NaF (0.0250 g, 0.6 mmol), and water (20 μL) were loaded into a 23-mL autoclave. The autoclave was sealed and heated to 220 °C in a box furnace for 5 days. The autoclave was then cooled to room temperature at a rate of 5 °C/h. The products were washed with boiling water to remove excess boric acid, followed by rinsing with methanol. Crystals in the form of tablets with yellow-green coloration were collected for **NaUBOF-1** with other light-yellow amorphous phases as side products. **NaUBOF-1** can be made from the reaction of $UO_2(NO_3)_2\cdot 6H_2O$, boric acid, NaF at different NaF:U:B molar ratios of 1:1:8, 1:1:15, 3:1:8, and 3:1:15, but none of these reactions yield a pure **NaUBOF-1** phase.

Synthesis of $K[(UO_2)B_5O_8(OH)F]$ (KUBOF-1) and $K_{11}[(UO_2)_6B_{24}O_{36}F_{22})](H_2BO_3)$ (KUBOF-2). $UO_2(NO_3)_2\cdot 6H_2O$, H_3BO_3, KF with eight different KF:U:B molar ratios (4:1:8, 4:1:15, 5:1:8, 5:1:15, 6:1:15, 8:1:15, 10:1:15, and 12:1:15) (0.1 g, 0.2 mmol of $UO_2(NO_3)_2\cdot 6H_2O$ for each reaction) and 20 μL of water were loaded into eight 23-mL autoclaves. The autoclaves were sealed and heated to 220 °C in a box furnace for 5 days. The autoclaves were then cooled to room temperature at a rate of 5 °C/h. All the products were washed with boiling water to remove excess boric acid, followed by rinsing with methanol. Crystals in the form of tablets and colorless glass phase were found for all reactions, and additional prismlike crystals were only found in the 8:1:15 reaction. Single-crystal X-ray diffraction (XRD) studies reveal that the tablet crystals are **KUBOF-1** and the prism crystals are **KUBOF-2**.

Synthesis of $Rb[(UO_2)B_5O_8(OH)F]$ (RbUBOF-1). **RbUBOF-1** can be prepared using $UO_2(NO_3)_2\cdot 6H_2O$, H_3BO_3, and $RbF\cdot xH_2O$ at different RbF:U:B molar ratios of 4:1:15, 6:1:15, and 8:1:15 by following the similar procedure for making the **NaUBOF-1**. Yellow-green crystals in the form of tablets were collected for **RbUBOF-1** with both light-yellow and colorless amorphous phases as side products for all the reactions. A pure phase of **RbUBOF-1** was not achieved.

Synthesis of $Tl[(UO_2)B_5O_8(OH)F]$ (TlUBOF-1). **TlUBOF-1** can be prepared using $UO_2(NO_3)_2\cdot 6H_2O$, H_3BO_3, TlF at different TlF:U:B molar ratios of 1:1:15, 1:1:22, 3:1:8, 3:1:15, and 3:1:22 by following the similar procedure for making the **NaUBOF-1**. Light yellow crystals of **TlUBOF-1** in the form of prisms were collected as a pure phase only in the 1:1:22 reaction with the yield of 29%, based on uranium. Colorless and yellow amorphous phases were found in all other reactions.

Synthesis of $Na[(NpO_2)B_5O_8(OH)F]\cdot H_2O$ (NaNpBOF-1). A 0.372 M stock solution of neptunium(VI) nitrate was prepared by first digesting 60 mg of NpO_2 in 8 M HNO_3 for 3 days at 200 °C in an autoclave. The resulting solution was reduced to a residue, during which all neptunium is oxidized to neptunium(VI). The residue was redissolved in 600 μL of water to form a 0.372 M stock solution of neptunium(VI) nitrate. One hundred microliters (100 μL) of neptunium(VI) nitrate stock solution was loaded into a 10-mL-volume PTFE autoclave (linear) and then heated at 140 °C to be reduced to a droplet. NaF (3.07 mg, 0.073 mmol) and a large excess of H_3BO_3 (47.2 mg, 0.77 mmol) were added to the droplet in the autoclave followed by the similar procedure for making the **NaUBOF-1**. Dark-green crystals of **NaNpBOF-1** in the form of tablets were collected with brown and colorless amorphous phases as side products.

Crystallographic Studies. Single crystals of all six actinide fluoroborate phases were mounted on glass fibers and optically aligned on a Bruker APEXII CCD X-ray diffractometer or a Bruker APEXII Quazar X-ray diffractometer, using a digital camera. Initial intensity measurements were either performed using a IμS X-ray source, a 30-W microfocused sealed tube (Mo Kα, $\lambda = 0.71073$ Å) with high-brilliance and high-performance focusing Quazar multilayer optics, or a standard sealed tube with a monocapillary collimator. APEXII software was used for determination of the unit cells and data collection control. The intensities of reflections of a sphere were collected by a combination of four sets of exposures (frames). Each set had a different φ angle for the crystal and each exposure covered a range of 0.5° in ω. A total of 1464

Table 1. Crystallographic Data for $Na[(UO_2)B_5O_8(OH)F]\cdot H_2O$ (NaUBOF-1), $K[(UO_2)B_5O_8(OH)F]$ (KUBOF-1), $K_{11}[(UO_2)_6B_{24}O_{36}F_{22})](H_2BO_3)$ (KUBOF-2), $Rb[(UO_2)B_5O_8(OH)F]$ (RbUBOF-1), $Tl[(UO_2)B_5O_8(OH)F]$ (TlUBOF-1), and $Na[(NpO_2)B_5O_8(OH)F]\cdot H_2O$ (NaNpBOF-1)

	Value/Comment					
parameter	NaUBOF-1	KUBOF-1	KUBOF-2	RbUBOF-1	TlUBOF-1	NaNpBOF-1
mass	526.07	526.18	3362.53	572.55	691.45	525.04
color and habit	yellow-green, tablet	yellow-green, prism	yellow-green, tablet	yellow-green, tablet	light-yellow, tablet	dark-green, tablet
space group	*Cc*	$P2_1/n$	$P6_3/m$	*Cc*	*P*1	*Cc*
a (Å)	11.1850(18)	6.443(2)	11.0914(8)	11.1442(16)	6.4163(11)	11.1753(16)
b (Å)	6.4007(10)	13.439(5)	11.0914(8)	6.4828(9)	6.4663(11)	6.3975(9)
c (Å)	14.191(2)	10.799(3)	26.577(3)	13.874(2)	7.1357(12)	14.113(2)
α (deg)	90	90	90	90	103.275(2)	90
β (deg)	104.634(2)	90.625(7)	90	95.462(2)	92.053(2)	104.930(2)
γ (deg)	90	90	120	90	119.580(2)	90
V (Å^3)	983.0(3)	935.1(5)	2831.4(4)	997.8(2)	246.67(7)	974.9(2)
Z	4	4	2	4	1	4
T (K)	100(2)	100(2)	100(2)	100(2)	100(2)	100(2)
λ (Å)	0.71073	0.71073	0.71073	0.71073	0.71073	0.71073
maximum 2*θ* (deg)	27.55	27.46	26.46	27.52	27.60	27.56
ρ_{calcd} (g cm^{-3})	3.555	3.738	3.944	3.811	4.655	3.577
μ(Mo Kα)	166.39	178.77	181.04	211.83	327.73	107.87
$R(F)$ for $F_o^2 > 2\sigma(F_o^2)$[a]	0.0164	0.0249	0.0262	0.0136	0.0294	0.0168
$Rw(F_o^2)$[b]	0.0347	0.0555	0.0501	0.0328	0.0540	0.0345

[a] $R(F) = \Sigma||F_0| - |F_c||/\Sigma|F_0|$ [b] $R(F_0^2) = [\Sigma w(F_0^2 - F_c^2)^2/\Sigma w(F_0^4)]^{1/2}$

Table 2. Selected Bond Distances for $Na[(UO_2)B_5O_8$-$(OH)F]\cdot H_2O$ (NaUBOF-1)

bond pair	distance (Å)	bond pair	distance (Å)
U(1)−O(7)	1.745(5)	B(1)−F(1)	1.429(5)
U(1)−O(6)	1.784(3)	B(1)−O(9)	1.457(6)
U(1)−O(10)	2.376(3)	B(1)−O(4)	1.457(5)
U(1)−O(9)	2.416(3)	B(1)−O(3)	1.492(6)
U(1)−O(4)	2.442(3)	B(2)−O(10)	1.459(5)
U(1)−O(2)	2.510(3)	B(2)−O(9)	1.471(5)
U(1)−O(3)	2.560(3)	B(2)−O(8)	1.476(5)
U(1)−O(5)	2.632(3)	B(2)−O(5)	1.482(5)
		B(3)−O(10)	1.464(5)
		B(3)−O(1)	1.467(5)
		B(3)−O(2)	1.469(5)
		B(3)−O(4)	1.484(5)
		B(4)−O(5)	1.356(5)
		B(4)−O(3)	1.366(6)
		B(4)−O(2)	1.377(5)
		B(5)−O(8)	1.364(5)
		B(5)−O(1)	1.364(6)
		B(5)−O(11)	1.386(6)

Table 3. Selected Bond Distances for $K[(UO_2)B_5O_8(OH)F]$ (KUBOF-1)

bond pair	distance (Å)	bond pair	distance (Å)
U(1)−O(8)	1.748(4)	B(1)−F(1)	1.398(8)
U(1)−O(6)	1.775(4)	B(1)−O(4)	1.461(8)
U(1)−O(1)	2.390(4)	B(1)−O(3)	1.461(8)
U(1)−O(3)	2.403(4)	B(1)−O(2)	1.495(8)
U(1)−O(4)	2.420(4)	B(2)−O(11)	1.357(8)
U(1)−O(5)	2.532(4)	B(2)−O(10)	1.368(8)
U(1)−O(2)	2.544(4)	B(2)−O(9)	1.370(8)
U(1)−O(7)	2.628(4)	B(3)−O(7)	1.351(7)
		B(3)−O(2)	1.372(8)
		B(3)−O(5)	1.377(8)
		B(4)−O(10)	1.462(8)
		B(4)−O(7)	1.464(8)
		B(4)−O(1)	1.464(7)
		B(4)−O(3)	1.476(8)
		B(5)−O(11)	1.441(8)
		B(5)−O(1)	1.465(7)
		B(5)−O(5)	1.466(7)
		B(5)−O(4)	1.486(7)

frames were collected with an exposure time of 10−80 s per frame, depending on the crystals. SAINT was used for data integration, including Lorentz and polarization corrections. Semiempirical absorption corrections were applied using the SADABS program.[31] Selected crystallographic data and bond distances information are listed in Tables 1−7. Atomic coordinates and additional structural information are provided in the Supporting Information (CIF files). The assignment of the F sites is challenging, because of the almost-identical scattering of oxygen and fluorine. Four lines of evidence support our assignments. First, B−F and B−O bonds are slightly different in length. Second, when the sites that we have assigned as fluoride are replaced with oxygen, the thermal parameter becomes nonpositive definite. Third, energy-dispersive X-ray (EDX) analysis has been used to measure the amount of fluoride in the crystals, and the An/F ratios from EDX are consistent with the formula derived from the crystal structures. Finally, the structures are different from compounds that lack fluoride.

dx.doi.org/10.1021/cm2004984 |*Chem. Mater.* 2011, 23, 2931–2939

Table 4. Selected Bond Distances for $K_{11}[(UO_2)_6B_{24}O_{36}F_{22})]\cdot(H_2BO_3)$ (KUBOF-2)

bond pair	distance (Å)	bond pair	distance (Å)
U(1)−O(5)	1.763(3)	B(1)−F(5)	1.448(11)
U(1)−O(3)	1.775(3)	B(1)−O(1)	1.451(4)
U(1)−O(8)	2.398(3)	B(1)−O(1)	1.451(4)
U(1)−O(4)	2.427(3)	B(1)−O(1)	1.451(4)
U(1)−O(1)	2.461(3)	B(2)−F(2)	1.456(10)
U(1)−O(7)	2.462(3)	B(2)−O(2)	1.464(4)
U(1)−O(2)	2.481(3)	B(2)−O(2)	1.464(4)
U(1)−O(6)	2.579(3)	B(2)−O(2)	1.464(4)
		B(3)−F(3)	1.432(7)
		B(3)−O(1)	1.443(6)
		B(3)−O(4)	1.456(6)
		B(3)−O(8)	1.462(6)
		B(4)−O(4)	1.447(7)
		B(4)−F(4)	1.449(7)
		B(4)−O(7)	1.456(6)
		B(4)−O(6)	1.480(6)
		B(5)−F(1)	1.414(6)
		B(5)−O(2)	1.461(6)
		B(5)−O(8)	1.462(7)
		B(5)−O(7)	1.480(6)
		B(6)−O(6)	1.367(3)
		B(6)−O(6)	1.367(3)
		B(6)−O(6)	1.367(3)
		B(7)−O(9)	1.380(4)
		B(7)−O(9)	1.380(4)
		B(7)−O(9)	1.380(4)

Table 5. Selected Bond Distances for $Rb[(UO_2)B_5O_8(OH)F]$ (RbUBOF-1)

bond pair	distance (Å)	bond pair	distance (Å)
U(1)−O(9)	1.769(5)	B(1)−O(1)	1.453(6)
U(1)−O(10)	1.762(5)	B(1)−O(4)	1.457(6)
U(1)−O(6)	2.394(3)	B(1)−O(6)	1.476(6)
U(1)−O(3)	2.427(3)	B(1)−O(7)	1.497(6)
U(1)−O(4)	2.432(3)	B(2)−O(7)	1.359(5)
U(1)−O(2)	2.552(3)	B(2)−O(2)	1.366(6)
U(1)−O(7)	2.591(3)	B(2)−O(11)	1.369(6)
U(1)−O(11)	2.610(3)	B(3)−F(1)	1.425(6)
		B(3)−O(3)	1.447(6)
		B(3)−O(2)	1.471(6)
		B(3)−O(4)	1.483(6)
		B(4)−O(8)	1.460(6)
		B(4)−O(6)	1.468(6)
		B(4)−O(11)	1.477(6)
		B(4)−O(3)	1.486(7)
		B(5)−O(1)	1.363(6)
		B(5)−O(8)	1.366(6)
		B(5)−O(5)	1.392(7)

Powder X-ray Diffraction. Powder X-ray diffraction (XRD) patterns of the products of pure **TlUBOF-1** reaction was collected on a Bruker powder diffractometer with a Lynxeye one-dimensional detector at room temperature in the angular range of 5°−80° (2θ), with a scanning step width of 0.05° 2θ and a fixed counting time of 1 s/step. The collected patterns were compared with those calculated from single-crystal data, using ATOMS, shown in the Supporting Information.

Table 6. Selected Bond Distances for $Tl[(UO_2)B_5O_8(OH)F]$ (TlUBOF-1)

bond pair	distance (Å)	bond pair	distance (Å)
U(1)−O(7)	1.759(6)	B(1)−O(8)	1.344(14)
U(1)−O(4)	1.768(6)	B(1)−O(10)	1.364(13)
U(1)−O(11)	2.392(7)	B(1)−O(9)	1.382(11)
U(1)−O(5)	2.423(6)	B(2)−O(1)	1.349(11)
U(1)−O(6)	2.425(6)	B(2)−O(2)	1.361(12)
U(1)−O(1)	2.566(6)	B(2)−O(3)	1.372(12)
U(1)−O(2)	2.581(6)	B(3)−O(11)	1.437(12)
U(1)−O(3)	2.604(7)	B(3)−O(3)	1.466(11)
Tl(1)−O(9)	2.721(6)	B(3)−O(9)	1.479(12)
Tl(1)−O(10)	2.764(6)	B(3)−O(6)	1.499(13)
		B(4)−F(1)	1.421(11)
		B(4)−O(6)	1.454(12)
		B(4)−O(5)	1.466(11)
		B(4)−O(2)	1.507(12)
		B(5)−O(5)	1.445(12)
		B(5)−O(10)	1.471(12)
		B(5)−O(1)	1.478(12)
		B(5)−O(11)	1.496(10)

Table 7. Selected Bond Distances for $Na[(NpO_2)B_5O_8(OH)F]\cdot H_2O$ (NaNpBOF-1)

bond pair	distance (Å)	bond pair	distance (Å)
Np(1)−O(11)	1.762(11)	B(1)−O(7)	1.362(7)
Np(1)−O(1)	1.749(11)	B(1)−O(9)	1.362(7)
Np(1)−O(8)	2.373(3)	B(1)−O(4)	1.371(7)
Np(1)−O(6)	2.405(4)	B(2)−O(8)	1.451(7)
Np(1)−O(3)	2.449(3)	B(2)−O(4)	1.466(7)
Np(1)−O(4)	2.516(4)	B(2)−O(10)	1.470(7)
Np(1)−O(7)	2.550(4)	B(2)−O(3)	1.479(7)
Np(1)−O(9)	2.640(4)	B(3)−O(5)	1.362(6)
		B(3)−O(10)	1.377(7)
		B(3)−O(2)	1.389(7)
		B(4)−O(6)	1.463(7)
		B(4)−O(9)	1.468(7)
		B(4)−O(8)	1.468(7)
		B(4)−O(5)	1.493(7)
		B(5)−F(1)	1.431(7)
		B(5)−O(6)	1.456(7)
		B(5)−O(3)	1.462(7)
		B(5)−O(7)	1.495(8)

Scanning Electron Microscopy/Energy-Dispersive Spectroscopy (SEM/EDS). Scanning electron microscopy/energy-dispersive spectroscopy (SEM/EDS) images and data were collected using a LEO Model EVO 50 system with an Oxford INCA energy-dispersive spectometer. The energy of the electron beam was 29.02 kV, and the spectrum acquisition time was 120 s. All of the data were calibrated with standards, and all EDS results are provided in the Supporting Information. Fluorine was found in all phases. **KUBOF-2** showed a much higher

dx.doi.org/10.1021/cm2004984 |*Chem. Mater.* 2011, 23, 2931–2939

F/U ratio than all other phases, which coincides with the proposed formula of **KUBOF-2**.

UV−vis-NIR and Fluorescence Spectroscopy. UV−vis-NIR data were acquired from a single crystal of **NaNpBOF-1**, using a Craic Technologies microspectrophotometer. Crystals were placed on quartz slides under Krytox oil, and the data were collected from 500 nm to 1400 nm. Fluorescence data were obtained for all uranium phases, using 365-nm light for excitation (see Supporting Information).

Second-Harmonic Generation Measurements. Powder second-harmonic generation (SHG) measurements were performed on a Kurtz−Perry nonlinear optical system.[32] A Q-switched Nd:YAG laser (Continuum Surelite I-10), operated at 10 Hz, provided the 1064-nm light that was used for all measurements. The SHG intensity was recorded from a pure polycrystalline sample of **TlUBOF-1**. No index of refraction matching fluid was used in these experiments. The SHG light at 532 nm was collected in reflection, selected by a narrow band-pass interference filter (Pomfret) and detected by a photomultiplier tube (RCA 1P28). A near-normal-incidence beam splitter reflected a small fraction of the laser beam onto a pyroelectric detector (Molectron Model J3-05) that was used as a laser pulse energy monitor. A digital storage oscilloscope (Tektronix Model TDS 640A) signal averaged and recorded both the SHG and incident laser energy signals. The average laser power was measured separately with a calibrated Scientech volume absorber calorimeter. *As an important note for other investigators interested in the nonlinear optical properties of radioactive materials: The practice of grinding and sieving powders so that comparisons can be made with reference materials of similar particle size is unsafe. We ground and sieved a less-radioactive thorium compound inside a glovebox and then surveyed the interior of the glovebox. There was a uniform contamination of 50 dpm on every surface tested. We recommend discontinuation of this practice immediately. It is enough to say that there is or is not SHG activity. The magnitude is not important enough to risk the health of researchers.*

RESULTS AND DISCUSSION

Synthesis. The boric acid flux reactions of actinide(VI) nitrates with alkali metal or pseudo-alkali-metal fluorides is a facile way to prepare novel actinide fluoroborates. However, unlike the uranyl borate system, where Li, Cs, and Ag uranyl borates can be made,[20] the same effort to synthesize Li, Cs, and Ag uranyl fluoroborates was not successful. Also, compared to actinide borate systems, isolating pure phases is much more difficult in the actinide fluoroborate system; all the reactions tested failed to yield pure phases, except for one reaction with a specific stoichiometry that yielded a pure thallium uranyl fluoroborate, $Tl[(UO_2)B_5O_8(OH)F]$ (**TlUBOF-1**), as confirmed by powder XRD (see Supporting Information).

The B−F bonds were formed in situ during the boric acid flux reactions. It is surprising that actinide fluoride compounds were not formed since fluoride is a strong ligand for actinides in all oxidation states, according to the Pearson acid base concept, and actinide fluoride compounds in most oxidation states are well-known.[33] However, this can be explained by the fact that the bond dissociation energy of B−F bonds (732 kJ/mol) is considerably larger than U−F bonds (648 kJ/mol), which indicates that the actinide fluoroborate compounds with B−F bonds instead of U−F bonds are the thermodynamic products.

It is also interesting that, in $Na[(NpO_2)B_5O_8(OH)F]\cdot H_2O$ (**NaNpBOF-1**), neptunium retains the +6 oxidation state. In our previous report, we described the syntheses of $K_4(NpO_2)_{6.73}[B_{20}O_{36}(OH)_2]$ and $Ba_2(NpO_2)_{6.59}[B_{20}O_{36}(OH)_2]\cdot H_2O$, which contain neptunium(IV), neptunium(V), and neptunium(VI).[21] These compounds are synthesized by the reactions of neptunium(VI) nitrate with molten boric acid. When chloride is the only counterion in the reaction, $(NpO_2)_4[(NpO_2)_{6.73}B_{20}O_{36}(OH)_2]$ forms.[21] This demonstrates that neptunium(VI) is first reduced to neptunium(V), followed by disproportionation. We noted later, however, that, in order to retain neptunium in the +6 oxidation state, neptunium(VI) perchlorate could be used as the starting materials, where perchlorate is likely acting as an oxidant that prevents neptunium from being reduced from VI to V.[24] The neptunium(VI) fluoroborate, $Na[(NpO_2)B_5O_8(OH)F]\cdot H_2O$ (**NaNpBOF-1**) likely crystallizes more rapidly than the reduction of neptunium(VI) to neptunium(V) occurs.

Structure Descriptions and Topological Aspects. The crystal structures of all of these compounds contain layered motifs and are based on similar functional groups. U and Np atoms have similar oxygen coordination ($U(Np)O_8$) with a hexagonal bipyramidal geometry. The pyramids are based on axial uranyl/neptunyl groups (UO_2^{2+}/NpO_2^{2+}), and six O atoms coordinate the UO_2^{2+}/NpO_2^{2+} groups in the equatorial plane. The bond lengths of $U(Np)-O$ in UO_2^{2+} and NpO_2^{2+} groups are practically identical and in the range of 1.74−1.78 Å. The boron environments are more diverse than what were previously observed in the crystal structures of actinide borates.[7−24] The structures of **NaUBOF-1**, **KUBOF-1**, **RbUBOF-1**, **TlUBOF-1**, and **NaNpBOF-1** are based on the same oxo- and fluorooxo-boron groups: BO_3 triangles, and BO_4 and BO_3F tetrahedra (Figure 1). The crystal structure of **KUBOF-2** is quite different from other phases and is formed by two types of BO_3 triangles and one type of tetrahedron: the BO_3F fluorooxo group (Figure 2). The B−O bond distances in the BO_3 triangles of all obtained structures are in the normal range of 1.34−1.39 Å. Bond lengths in BO_4 tetrahedra are also standard, and range from 1.44 Å to 1.50 Å. The B−F bond lengths in **KUBOF-2** are in the range of 1.41−1.46 Å, which are slightly longer than those in the other phases, where the same bonds are in range of 1.40−1.43 Å. Such differences are probably a result of the different environment of the F atoms. In the structure of **KUBOF-2**, F atoms are contacted only with K atoms in the interlayer space, whereas, in all other compounds, the environments of the F atoms are more complicated, because the hydrogen bonding is involved. Based on the general aspects of the layered structures and organization of the interlayer space, we can separate the six actinide fluoroborate phases into three groups. The first group includes **NaUBOF-1**, **RbUBOF-1**, **TlUBOF-1**, and **NaNpBOF-1**, whereas the second and third groups have only one member each: **KUBOF-1** and **KUBOF-2**, respectively.

All compounds in the first group contain layers with the same type of topologies (A/B-type layers), which were first observed in sodium uranyl borates.[17] However, alternating orders and the orientations of these layers strongly vary among these phases, which leads to different space groups adopted by these phases (chiral, polar space group *P*1 for **TlUBOF-1** and noncentrosymmetric space group *Cc* for **NaUBOF-1**, **NaNpBOF-1**, and **RbUBOF-1**). The simplest one is **TlUBOF-1**, which is formed by only one type of layer (see Figure 1d). The layers are packed together without further rotation, which results in the unit cell with only one layer for **TlUBOF-1**. **NaUBOF-1** and **NaNpBOF-1** are isotypic and similar with **RbUBOF-1**. All of these phases are based on two types of alternating layers shown in Figures 1a and 1c. The only difference between **NaUBOF-1**/**NaNpBOF-1** and **RbUBOF-1** is the layer orientations. Each second layer is turned 120°, with respect to the nearest layer in structures of **NaUBOF-1** and **NaNpBOF-1**, whereas, in the structure of **RbUBOF-1**, the angle is only 60°. Also, the interlayer content is different, since the sodium phase is hydrated while the rubidium phase is anhydrous. Each layer in the structures of **NaUBOF-1**,

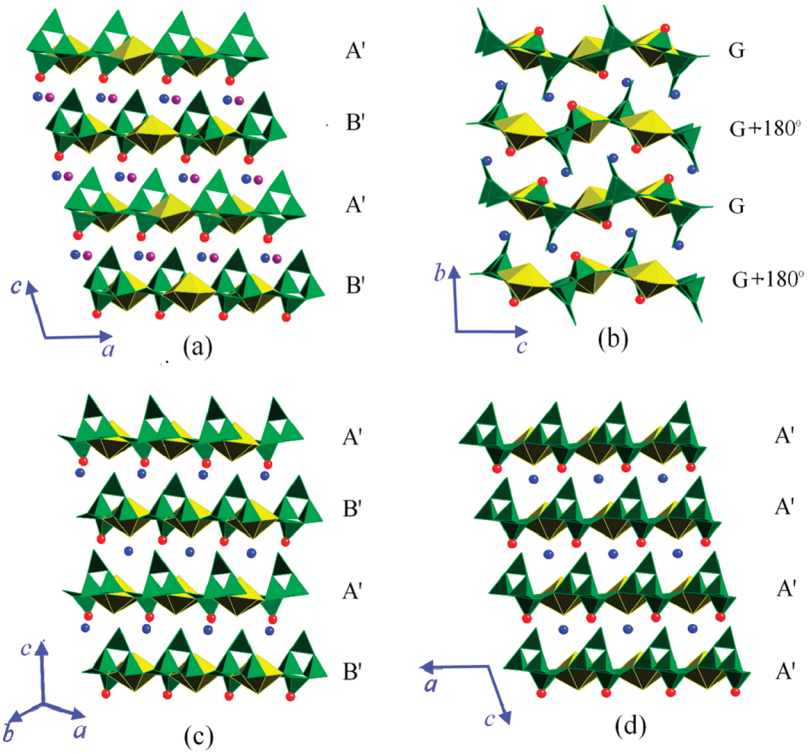

Figure 1. Fragments of (a) **NaUBOF-1** and **NaNpBOF-1**, (b) **KUBOF-1**, (c) **RbUBOF-1**, (d) **TlUBOF-1** crystal structures. (U atoms are shown in yellow and B atoms are shown in green; F, Na−Tl, and water molecules are shown as red, blue, and violet spheres, respectively.)

RbUBOF-1, **TlUBOF-1**, and **NaNpBOF-1** has "additional" BO_3 triangles perpendicular to the plane of the layer. The general topology of such layers is identical with α-$Na[(UO_2)_2B_{10}O_{15}(OH)_5]$, β-$Na[(UO_2)_2B_{10}O_{15}(OH)_5]$, $Na[(UO_2)_2B_{10}O_{15}(OH)_5]\cdot 3H_2O$, and $K[(UO_2)_2B_{10}O_{15}(OH)_5]$ and can be described with 1 L-1-0-0 descriptor.[20] However, the way the layers pack in the mentioned phases and in **NaUBOF-1**, **RbUBOF-1**, **TlUBOF-1**, and **NaNpBOF-1** is different. In the structures of α-$Na[(UO_2)_2B_{10}O_{15}(OH)_5]$, β-$Na[(UO_2)_2B_{10}O_{15}(OH)_5]$, $Na[(UO_2)_2B_{10}O_{15}(OH)_5]\cdot 3H_2O$, $K[(UO_2)_2B_{10}O_{15}(OH)_5]$, the layers are packed "face-to-face", which means "additional" BO_3 triangles in two nearest layers are directed toward each other. The bonding between them is provided by alkali-metal cations. The other sides of the layers that do not have "additional" BO_3 unit are also turned to each other but they are bound by strong hydrogen bonds provided by terminal B−OH groups. In the structures of **NaUBOF-1**, **RbUBOF-1**, **TlUBOF-1**, and **NaNpBOF-1**, these B−OH bonds are substituted by B−F bonds and hydrogen bonding disappears between these fragments. Thus, the orientation of the layers must be modified to provide the bonding via monovalence metal cations. The only way to achieve this is turning the sides of layers with "additional" BO_3 triangles to the sides with terminal B−F groups, which can be observed in **NaUBOF-1**, **RbUBOF-1**, **TlUBOF-1**, and **NaNpBOF-1**. Such modification is an example of how a new structure type is formed by functionalized structural units plus the old topology of main structural fragments.

The second group includes only one phase which is **KUBOF-1**. The layer topology is different from the A/B types observed in the phases of the first group. In general, the layers in **KUBOF-1** are very similar with the structure of silver uranyl borate ($Ag[(UO_2)B_5O_8(OH)_2]$, G-type layer topology) and can be described with 1 L-1-1-0 descriptor (see Figure 1b).[20] The corrugated layers of **KUBOF-1** are linked into a quasi-three-dimensional (3D) framework via K···O, K···F interactions and hydrogen bonds between terminal B−OH groups in additional BO_3 triangles perpendicular to the layers. The layer packing mode in **KUBOF-1** is also identical with the structure of $Ag[(UO_2)B_5O_8(OH)_2]$ and based on the same layer types (G-type) that rotate by 180° with respect to each other between neighboring layers (see Figure 1b). The G-type topology in the structure of **KUBOF-1** allowed the formation of symmetrical layers where terminal functional B−F groups appear on both sides of the layers. This makes the layers nonpolar, and the structural modifications that we observed in α-$Na[(UO_2)_2B_{10}O_{15}(OH)_5]$, β-$Na[(UO_2)_2B_{10}O_{15}(OH)_5]$, $Na[(UO_2)_2B_{10}O_{15}(OH)_5]\cdot 3H_2O$, $K[(UO_2)_2B_{10}O_{15}(OH)_5]$) → (**NaUBOF-1**, **RbUBOF-1**, **TlUBOF-1**, and **NaNpBOF-1**) are not required. Interestingly, **KUBOF-1** does not have an analogue in the group of potassium uranyl borates, including $K[(UO_2)_2B_{10}O_{15}(OH)_5]$, $K[(UO_2)_2B_{10}O_{16}(OH)_3]\cdot H_2O$, $K_2[(UO_2)_2B_{12}O_{19}(OH)_4]\cdot 0.3H_2O$.[17] This could be another effect of BO_4 to BO_3F tetrahedra modification. The K···F bonds are stronger than K···O interactions and helps with the stabilization of $Ag[(UO_2)B_5O_8(OH)_2]$ structure type with K^+ as an interlayer cation.

The third group also has only one member: **KUBOF-2**. The crystal structure of this phase is very unusual in all regards, which combines structural aspects from groups of uranyl borates obtained from both high- and mild-temperature synthetic methods. The general view of the **KUBOF-2** structure is shown in Figure 2a. The two-dimensional (2D) layered structure of **KUBOF-2** is based on BO_3 triangles appearing only in the layers and BO_3F tetrahedra. The layers are asymmetric since, on one side, there are twice as many terminal B−F groups (Figure 2b) than the other side (Figure 2c). All of BO_4 tetrahedra were

dx.doi.org/10.1021/cm2004984 |*Chem. Mater.* 2011, 23, 2931–2939

substituted by BO_3F units in the layers of **KUBOF-2**, and there are no additional BO_3 groups oriented perpendicular to the layer planes. The structure can be described with a 1 L-0-0-0 descriptor.[20] This is the first difference between **KUBOF-2** and all other phases reviewed in this work. The second difference is the topology of fluorooxo-borate layers. In Figures 2b and 2c, triangles are shown in red, tetrahedra are in green, and we can observe only one BO_3 triangle and eight BO_3F tetrahedra around each UO_2^{2+} hexagonal bipyramid. This is the lowest BO_3/$BO_4(BO_3F)$ ratio observed to date in the actinide borate system.

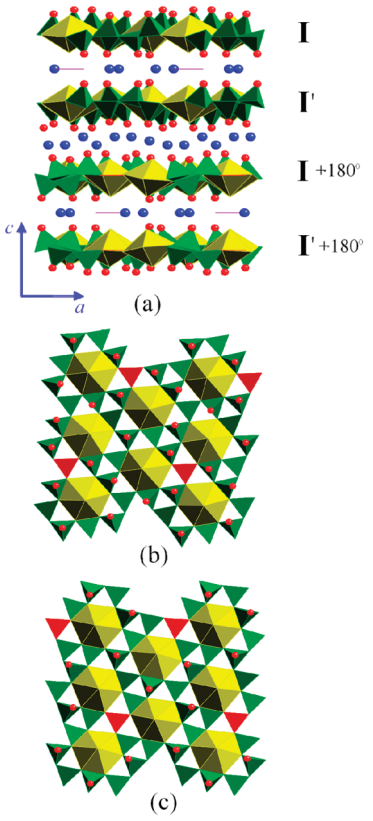

Figure 2. (a) Fragment of **KUBOF-2** crystal structure; (b and c) structures of layers in **KUBOF-2**. (U atoms are shown in yellow and B atoms are shown in green; F and K atoms are shown in red and blue, respectively. BO_3 groups (in layers) are shown as red triangles, and BO_3^{3-} anions are shown as violet lines.)

The layers observed in the structure of **KUBOF-2** are named as **I**-type. Skeletal representations of this layer topology are shown in Figures 3a (**I**-type) and 3b (**I′**-type). Three BO_3F tetrahedra are linked via vertices into supertriangle-like groups. Two of them are directed "up" (in **I**-type) or "down" (in **I′**-type), which provides the main difference between **I** and **I′** geometries and is very similar with orientations of the same supertriangles in **A**/**B**- and **A′**/**B′**-type layers.[17] The difference between **A**/**B**-types and **I**-type layers is in the method of the supertriangles linkage. The supertriangles in the structures of **A**/**B**-types layers are linked into 2D layers by BO_3 triangles only, while two-thirds of the BO_3 triangles are now substituted by BO_3F tetrahedra in **I**-type layers, as shown in Figures 3a and 3b. One of these BO_3F tetrahedra is directed "up" (shown in green in Figure 3a and blue in Figure 3b), while others are directed "down" (green in Figure 3a and blue in Figure 3b, respectively). **I**-type and **I′**-type layers are enantiomorphic and have the same symmetrical relationship, as we demonstrated in the **A**/**B**-type layers system.[17] Described layers alternate in the structure of **KUBOF-2** with the following packets: (**I**/**I′**)(**I** + **180°**/**I′** + **180°**)(**I**/**I′**) (see Figure 2a). The layers in each packet face each other via the side shown in Figure 2c. The layers from different packets face each other via the other side, which contains twice as many B−F groups on the surface (demonstrated in Figure 2b). This is the third difference between **KUBOF-2** and other phases discussed in this paper. Thus, we have two types of interlayer constituents, and the nature of these constituents is also different. There are only K^+ cations in the interlayer space between (**I**/**I′**) and (**I** + **180°**/**I′** + **180°**) packets (Figure 2a). These cations are connected only by F atoms (in the case of K1) or by F and O atoms from B−F groups and uranyl groups (in the case of K4). The interlayer content within packets consists of both K^+ cations and $H_2BO_3^-$ anions with a K:H_2BO_3 ratio of 4: 1 (see Figure 2a; $H_2BO_3^-$ anions are violet). The same anionic groups ($H_2BO_3^-$) were also found in the structure of $Th[B_5O_6(OH)_6](H_2BO_3)\cdot 2.5H_2O$ (**NDTB-1**), where it only appeared in the cages and channels.[15] The $H_2BO_3^-$ anions are located right on the top of BO_3 triangles from the neighboring layers within one package (coordinates *x*,*y*,*z*: B6 in $H_2BO_3^-$ anions, 0.33333,0.66667,−0.12018; B7 in the layers, 0.33333,0.66667, −0.25000) through the *c*-axis. The O atoms from $H_2BO_3^-$ are also bound to the K3 cations. It is impossible to localize of H^+ positions on the $H_2BO_3^-$ anions, since all these O atoms in the $H_2BO_3^-$ anions are crystallographically equivalent. Most probably, they are delocalized as an effect of $H_2BO_3^-$ rotations among equivalent structural positions. The structure of $Ni_7UB_4O_{16}$ shares certain

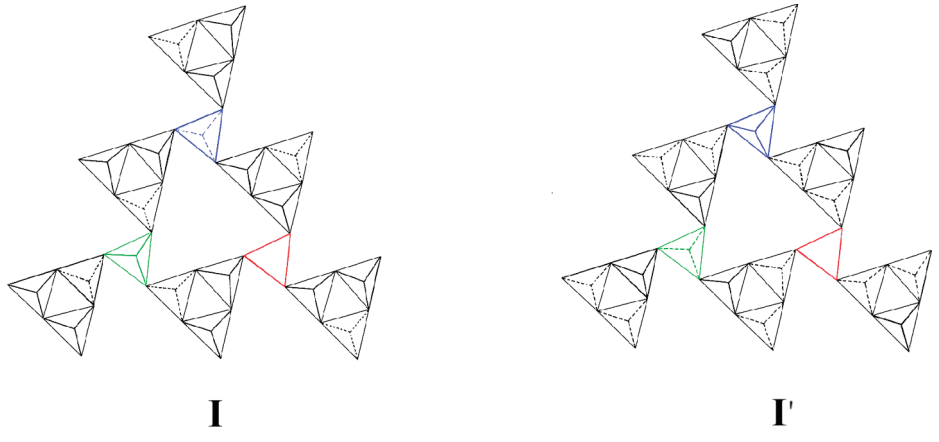

Figure 3. Schematic representation of layer topology in **KUBOF-2**. (See text for details.)

dx.doi.org/10.1021/cm2004984 |*Chem. Mater.* 2011, 23, 2931–2939

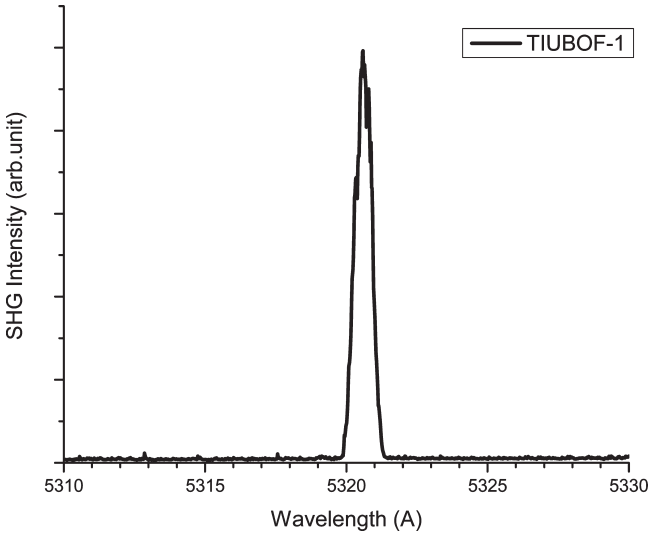

Figure 4. Second-harmonic generation (SHG) of 532-nm laser light from 1064-nm laser light obtained from the pure polycrystalline sample of **TlUBOF-1**.

similarities with **KUBOF-2**. There are both nickel cations and BO_3^{3-} anions between uranyl borate chains.[12] However, this phase was obtained by the high-temperature solid-state B_2O_3 flux reactions.

The structure of **KUBOF-2** is a logically final point in the process of borate network functionalization within uranyl borate layers. The replacement of all terminal O atoms with F atoms provides substantial changes in the structure formation, which leads to multifunctional interlayer contents.

Nonlinear Optical Properties. As mentioned above, the partial substitution of BO_4 by BO_3F tetrahedra can further reduce the symmetry. **TlUBOF-1** crystallizes in the chiral and polar space group *P*1 without any symmetry elements present in the crystal structure, and it is the only phase that can be obtained in pure form. Thus, this compound is capable of exhibiting a wide range of physical properties, including the second-harmonic generation (SHG) of light when irradiated with a high-wavelength near-infrared (NIR) laser. When a pure polycrystalline sample of **TlUBOF-1** is irradiated with 1064-nm light, a sharp strong signal with 532-nm light is clearly observed, as shown in Figure 4.

UV−vis-NIR Absorption Spectroscopy. Uranium(VI) compounds usually show charge-transfer bands in the UV region of the spectrum without f−f transitions, since there is no 5f electrons in uranium(VI), while neptunium(VI), which has a $5f^1$ electron configuration, yields a single broad Laporte-forbidden f−f transition in addition to higher-energy charge-transfer bands.[34] Typically, for neptunium(VI), this transition occurs in the NIR near 1200 nm.[34] The UV−vis−NIR spectrum of **NaNpBOF-1** acquired from a single crystal is shown in Figure 5, the transition is observed at 1120 nm. We again noted that this transition peak position is closely associated with the coordination geometries of neptunium(VI) when in the solid state. For example, as we previously observed, the f−f transition peak for single crystals of $NpO_2(NO_3)_2\cdot 6H_2O$ is located at 1100 nm and $NpO_2[B_8O_{11}(OH)_4]$ shows a transition at 1140 nm.[24] The transition of NpO_8 units are blue-shifted, compared to NpO_7 units.[24,35] In the higher-energy visible region, the fine vibronically coupled charge-transfer bands are shown for neptuyl units NpO_2^{2+}.[36]

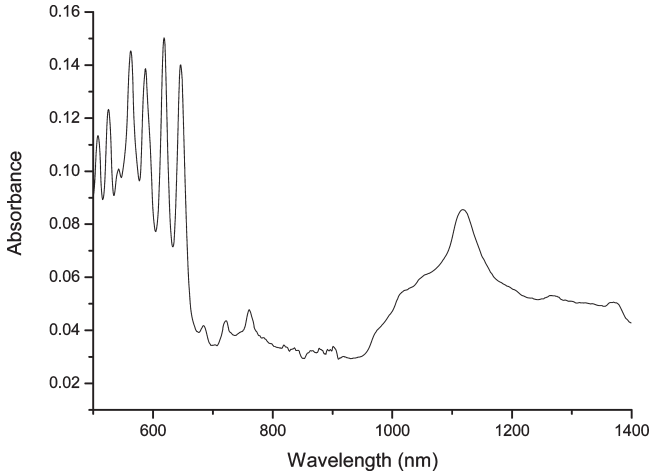

Figure 5. UV−vis−NIR absorption spectrum of a single crystal of $Na[(NpO_2)B_5O_8(OH)F]\cdot H_2O$ (**NaNpBOF-1**) showing both f−f transtion and vibronic-coupled charge-transfer bands.

Fluorescence Properties. Denning and co-workers have carefully and extensively studied the emission from uranyl compounds, and assigned all of the vibronic transitions from single crystals containing the $[UO_2Cl_4]^{2-}$ anion.[37] While five broad features centered near 520 nm are generally observed for uranyl compounds at room temperature, far more bands are resolved at low temperatures.

$Na[(UO_2)B_5O_8(OH)F]\cdot H_2O$ (**NaUBOF-1**), $K[(UO_2)B_5O_8(OH)F]$ (**KUBOF-1**), $K_{11}[(UO_2)_6B_{24}O_{36}F_{22})](H_2BO_3)$ (**KUBOF-2**), and $Rb[(UO_2)B_5O_8(OH)F]$ (**RbUBOF-1**) all form crystals with the pale yellow-green coloration. Upon irradiation with 365-nm light, these crystals fluoresce with sufficient intensity that the emission from a few crystals is easily observed by the naked eye. The fluorescence spectra are all provided in the Supporting Information. Given that all of the uranyl borates contain very similar site symmetry around the uranium atoms (D_{6h}), it is not surprising that they are all very similar to the alkali-metal uranyl borates that we synthesized.[17−20] However, $Tl[(UO_2)B_5O_8(OH)F]$ (**TlUBOF-1**) forms crystals with a light yellow coloration, and these crystals do not fluoresce when irradiated with 365-nm light. It is expected that the Tl^+ quenches the fluorescence features from the uranyl units, which has also been observed in all thallium uranyl borate compounds.[17,20]

■ CONCLUSIONS

In summary, we have demonstrated that the boric acid flux reactions of actinide starting materials with the alkali-metal or pseudo-alkali-metal fluorides is a facile method for preparing novel actinide fluoroborates containing the BO_3F unit. Compared with the actinide borate family, the modification of BO_4 to BO_3F tetrahedra further reduces the symmetry and improves the probability of achieving a noncentrosymmetric phase. Pure phases can be synthesized in this family through careful control of reaction composition. More importantly, the replacement of B−OH bonds with B−F bonds should substantially enhance the stability of these materials, and the borate networks can now be greatly modified to yield novel actinide borate layered topologies and layer packing modes that are further enrichments of the actinide borate system. Finally, as observed in **NaNpBOF-1**, the redox chemistry of transuranium elements is greatly affected by

counterions, and neptunium(VI) is stabilized in the presence of fluoride. Perhaps the greatest surprise in this family is the lack of U−F and Np−F bonds. B−F bonds are simply much stronger, and this is one of very few families of fluoride-containing compounds with actinides where An−F bonds do not occur. There are in fact other systems where fluoride could potentially be incorporated without forming An−F bonds. For example, the beryllium fluoroborate compounds, $ABe_2BO_3F_2$ (A = K, Rb, -Cs, Tl),[38] are among the best optical materials for deep UV applications.[39] In these compounds, B−F bonds do not exist, and the fluoride is solely bound to beryllium. Therefore, actinide compounds that contain both beryllium and fluoride may also lack An−F bonds. We will be exploring this system shortly.

■ ASSOCIATED CONTENT

Supporting Information. Fluorescence spectra for Na-$[(UO_2)B_5O_8(OH)F]\cdot H_2O$ (**NaUBOF-1**), $K[(UO_2)B_5O_8(OH)F]$ (**KUBOF-1**), $K_{11}[(UO_2)_6B_{24}O_{36}F_{22})](H_2BO_3)$ (**KUBOF-2**), $Rb[(UO_2)B_5O_8(OH)F]$ (**RbUBOF-1**); X-ray files (CIF) for Na-$[(UO_2)B_5O_8(OH)F]\cdot H_2O$ (**NaUBOF-1**), $K[(UO_2)B_5O_8(OH)F]$ (**KUBOF-1**), $K_{11}[(UO_2)_6B_{24}O_{36}F_{22})](H_2BO_3)$ (**KUBOF-2**), Rb-$[(UO_2)B_5O_8(OH)F]$ (**RbUBOF-1**), $Tl[(UO_2)B_5O_8(OH)F]$ (**TlUBOF-1**), and $Na[(NpO_2)B_5O_8(OH)F]\cdot H_2O$ (**NaNpBOF-1**). This material is available free of charge via the Internet at http://pubs.acs.org.

■ AUTHOR INFORMATION

Corresponding Author

*Tel.: 574-631-1872. Fax: 574-631-9236. E-mail: talbrec1@nd.edu.

■ ACKNOWLEDGMENT

We are grateful for support provided by the Chemical Sciences, Geosciences, and Biosciences Division, Office of Basic Energy Sciences, Office of Science, Heavy Elements Program, U.S. Department of Energy (under Grant No. DE-SC0002215). This material is based upon work supported as part of the Materials Science of Actinides, an Energy Frontier Research Center funded by the U.S. Department of Energy, Office of Science, Office of Basic Energy Sciences (under Award No. DE-SC0001089).

■ REFERENCES

(1) (a) Chen, C.; Wu, B.; Jiang, A.; You, G. *Sci. Sinica B* **1984**, *B7*, 598. (b) Chen, C.; Wu, Y.; Jiang, A.; Wu, B.; You, G.; Li, R.; Lin, S. *J. Opt. Soc. Am. B.* **1989**, *6*, 616. (c) Chen, C.; Wang, Y.; Wu, B.; Wu, K.; Zeng, W.; Yu, L. *Nature* **1995**, *373*, 322. (d) Pan, S.; Wu, Y.; Fu, P.; Zhang, G.; Li, Z.; Du, C.; Chen, C. *Chem. Mater.* **2003**, *15*, 2218.

(2) Hellwig, H.; Liebertz, J.; Bohaty, L. *Solid State Commun.* **1998**, *109*, 249.

(3) Huppertz, H.; von der Eltz, B. *J. Am. Chem. Soc.* **2002**, *124*, 9376.

(4) Jin, S.; Cai, G.; Wang, W.; He, M.; Wang, S.; Chen, X. *Angew. Chem., Int. Ed.* **2010**, *49*, 4967.

(5) (a) Burns, P. C.; Grice, J. D.; Hawthorne, F. C. *Can. Mineral.* **1995**, *33*, 1131. (b) Grice, J. D.; Burns, P. C.; Hawthorne, F. C. *Can. Mineral.* **1999**, *37*, 731.

(6) (a) Yuan, G.; Xue, D. *Acta Crystallogr., Sect. B: Struct. Sci.* **2007**, *B63*, 353. (b) Belokoneva, E. L. *Cryst. Res. Technol.* **2008**, *43*, 1173. (c) Touboul, M.; Penin, N.; Nowogrocki, G. *Solid State Sci.* **2003**, *5*, 1327.

(7) Behm, H. *Acta Crystallogr., Sect. C: Cryst. Struct. Commun.* **1985**, *C41*, 642.

(8) Gasperin, M. *Acta Crystallogr., Sect. C: Cryst. Struct. Commun.* **1987**, *C43*, 1247.

(9) Gasperin, M. *Acta Crystallogr., Sect. C: Cryst. Struct. Commun.* **1987**, *C43*, 2031.

(10) Gasperin, M. *Acta Crystallogr., Sect. C: Cryst. Struct. Commun.* **1987**, *C43*, 2264.

(11) Gasperin, M. *Acta Crystallogr., Sect. C: Cryst. Struct. Commun.* **1988**, *C44*, 415.

(12) Gasperin, M. *Acta Crystallogr., Sect. C: Cryst. Struct. Commun.* **1989**, *C45*, 981.

(13) Gasperin, M. *Acta Crystallogr., Sect. C: Cryst. Struct. Commun.* **1990**, *C46*, 372.

(14) Gasperin, M. *Acta Crystallogr., Sect. C: Cryst. Struct. Commun.* **1991**, *C47*, 10.

(15) Wang, S.; Alekseev, E. V.; Diwu, J.; Casey, W. H.; Phillips, B. L.; Depmeier, W.; Albrecht-Schmitt, T. E. *Angew. Chem., Int. Ed.* **2010**, *49*, 1057.

(16) Yu, P.; Wang, S.; Alekseev, E. V.; Depmeier, W.; Albrecht-Schmitt, T. E.; Phillips, B.; Casey, W. *Angew. Chem., Int. Ed.* **2010**, *49*, 5975.

(17) Wang, S.; Alekseev, E. V.; Ling, J.; Liu, G.; Depmeier, W.; Albrecht-Schmitt, T. E. *Chem. Mater.* **2010**, *22*, 2155.

(18) Wang, S.; Alekseev, E. V.; Stritzinger, J. T.; Depmeier, W.; Albrecht-Schmitt, T. E. *Inorg. Chem.* **2010**, *49*, 2948.

(19) Wang, S.; Alekseev, E. V.; Stritzinger, J. T.; Depmeier, W.; Albrecht-Schmitt, T. E. *Inorg. Chem.* **2010**, *49*, 6690.

(20) Wang, S.; Alekseev, E. V.; Stritzinger, J. T.; Liu, G.; Depmeier, W.; Albrecht-Schmitt, T. E. *Chem. Mater.* **2010**, *22*, 5983.

(21) Wang, S.; Alekseev, E. V.; Ling, J.; Skanthakumar, S.; Soderholm, L.; Depmeier, W.; Albrecht-Schmitt, T. E. *Angew. Chem., Int. Ed.* **2010**, *49*, 1263.

(22) Wang, S.; Alekseev, E. V.; Depmeier, W.; Albrecht-Schmitt, T. E. *Chem. Commun.* **2010**, *46*, 3955.

(23) Wang, S.; Alekseev, E. V.; Miller, H. M.; Depmeier, W.; Albrecht-Schmitt, T. E. *Inorg. Chem.* **2010**, *49*, 9755.

(24) Wang, S.; Villa, E. M.; Diwu, J.; Alekseev, E. V.; Depmeier, W.; Albrecht-Schmitt, T. E. *Inorg. Chem.* **2011**, *50*, 2527.

(25) Chackraburtty, D. M. *Acta Crystallogr.* **1957**, *10*, 199.

(26) Huang, Y.-X.; Schafer, G.; Borrmann, H.; Zhao, J.-T.; Kniep, R. *Z. Anorg. Allg. Chem.* **2003**, *629*, 3.

(27) Li, M.-R.; Liu, W.; Ge, M.-H.; Chen, H.-H.; Yang, X.-X.; Zhao, J.-T. *Chem. Commun.* **2004**, *11*, 1272.

(28) Lieb, A.; Weller, M. T. *Z. Anorg. Allg. Chem.* **2009**, *635*, 1877.

(29) Li, L.; Li, G.; Wang, Y.; Liao, F.; Lin, J. *Chem. Mater.* **2005**, *17*, 4174.

(30) Cakmak, G.; Nuss, J.; Jansen, M. *Z. Anorg. Allg. Chem.* **2009**, *635*, 631.

(31) (a) Sheldrick, G. M. SADABS 2001, Program for absorption correction using SMART CCD based on the method of Blessing: (b) Blessing, R. H. *Acta Crystallogr., Sect. A: Found Crystallogr.* **1995**, *A51*, 33.

(32) Kurtz, S. K.; Perry, T. T. *J. Appl. Phys.* **1968**, *39*, 3798.

(33) (a) Kern, S.; Hayward, J.; Roberts, S.; Richardson, J. W., jr.; Rotella, F. J.; Soderholm, L.; Cort, B.; Tinkle, M.; West, M.; Hoisington, D.; Lander, G. H. *J. Chem. Phys.* **1994**, *101*, 9333. (b) Levy, J. H.; Taylor, J. C.; Waugh, A. B. *J. Fluorine Chem.* **1983**, *23*, 29. (c) Howard, C. J.; Taylor, J. C.; Waugh, A. B. *J. Solid State Chem.* **1982**, *45*, 396. (d) Staritzky, E.; Douglass, R. M. *Anal. Chem.* **1956**, *28*, 1056.

(34) Liu, G.; Beitz, J. V. in *The Chemistry of the Actinide and Transactinide Elements*; Springer: Dordrecht, The Netherlands, 2006; Vol. 3, pp 2013−2111.

(35) Bean, A. C.; Scott, B. L.; Albrecht-Schmitt, T. E.; Runde, W. *Inorg. Chem.* **2003**, *42*, 5632.

(36) Wilkerson, M. P.; Berg, J. M.; Hopkins, T. A.; Dewey, H. J. *J. Solid State Chem.* **2005**, *178*, 584.

(37) Denning, R. G.; Norris, J. O. W.; Short, I. G.; Snellgrove, T. R.; Woodwark, D. R. *Lanthanide and Actinide Chemistry and Spectroscopy*; ACS Symposium Series No. 131; Edelstein, N. M., Ed.; American Chemical Society: Washington, DC, 1980; Chapter 15.

(38) McMillen, C. D.; Hu, J.; VanDerveer, D.; Kolis, J. W. *Acta Crystallogr., Sect. B: Struct. Sci.* **2009**, *B65*, 445.

(39) Kanai, T.; Wang, X.; Adachi, S.; Watanabe, S.; Chen, C. *Opt. Express* **2009**, *17*, 8696.